Indian Journal of Pure & Applied Physics
Vol. 56, December 2018, pp. 978-988

Dielectric relaxation and modulus studies of PEO-PAM blend based sodium salt electrolyte system

G Dave & D K Kanchan*

Solid State Ionics & Glass Research Laboratory, Physics Department, Faculty of Science,
The M S University of Baroda, Vadodara 390 002, India

Received 21 November 2017; accepted 19 June 2018

Dielectric properties of solid polymer electrolyte having PEO-PAM blend matrix with sodium trifluoromethane sulfonate ($NaCF_3SO_3$) as ionic salt have been studied. The samples have been prepared by solution cast technique. X-ray diffraction analysis has been carried to understand the formation of blend, complexation and crystallinity of the polymer blend with the variation of salt amount. Complex impedance spectroscopy has been used to study ionic conductivity, dielectric relaxation and modulus formalism as a function of frequency at various temperatures. Scaling of M'' spectra has been carried out and it has been found that the dynamic relaxation processes occurring in the system are dependent on temperature as well as salt concentration. Highest conductivity at room temperature has been found to be 2.81×10^{-7} S/cm for sample with 17.5 wt% $NaCF_3SO_3$.

Keywords: Blend polymer electrolyte, Sodium triflate, Dielectric relaxation, Modulus formalism

1 Introduction

Solid polymer electrolytes (SPE) have been studied continuously since more than two decades for their conceivable applications in electrochemical devices such as solid state batteries and super capacitors. Wright[1] reported high conductivity for alkali metal salt complexes with solid polymer electrolytes. High molecular weight PEO (polyethylene oxide) based polymer electrolytes have been materialized as the most suitable host matrix. Polymer blending has been realized as one of the most promising technique for reducing the crystalline phase of PEO and obtaining a host matrix with better properties. The amorphous region of the polymers is enhanced by polymer blending which results in overall good conductivity of the electrolyte system[2]. Blends of PEO with other polymers have been reported[3-7]. PAM (polyacrylamide) is largely amorphous in nature and commonly used matrix for nano-composite hydrogels[8]. PAM and PEO are both water soluble neutral pH polymers and harmonious with different electrode and current collector materials[9]. Generally, if a blend of PEO:PAM-salt is prepared, it may contain pure PEO crystalline regions, salt rich crystalline regions and amorphous regions formed out of PEO:PAM-salt complexation. The polymer crystalline regions exhibit limited free space between and along the polymeric chains and produce restricted segmental motion of the polymeric chains. On the other hand, the free space in the amorphous region contributes to the mobility of ions supported by segmental motion of the polymeric chains in electrolyte systems. Thus, transport of ions in PEO: PAM blend systems is expected to be easier due to enhanced amorphous content in the system controlling the ionic conductivity[10].

Lithium salt[11-13] based polymer electrolytes have been extensively used in battery applications since a long time. Lithium based compounds are very hazardous and the limited sources of lithium metal are not enough[14,15]. Studies on conducting property of Na place it as a potential alternative to Li salt[10,16-19]. Sodium has very well established itself as a competent candidate as compared to other metal ion electrolytes due to its material abundance, low cost and environment friendly nature[15,20-22].

Understanding the electrochemical properties of blend of PAM with PEO and sodium triflate as a salt will make an interesting and a thought-provoking study. Therefore, in the present study, we have discussed the dielectric relaxation behavior and modulus formalism of sodium-ion in the blend of PEO and PAM polymers.

*Corresponding author (E-mail: dkkanchan.ssi@gmail.com)

2 Experimental

Polyacrylamide (PAM; molecular weight =50,00,000 $gmol^{-1}$) from Hi-Media, polyethylene oxide (PEO; molecular weight = 300,000 $gmol^{-1}$) from Alfa Aesar and sodium trifluoromethanesulfonate ($NaCF_3SO_3$) from Sigma Aldrich are obtained. All chemicals are used as received. For preparing blend polymer electrolytes, both polymers PEO and PAM were taken in (1:1) ratio by weight. Concentration of the salt (***C***) is also taken in weight ratios of the total polymer system as 5, 7.5, 10, 12.5, 15 and 17.5. Polymers and the salt as a whole are dissolved in deionized water and stirred for 24 h continuously to achieve a homogeneous mixture. Solutions thus prepared with different amounts of salt are solution casted into Teflon petri dish. Free standing films of 160-220 μm thickness have been obtained after evaporating all traces of solvent at room temperature. The obtained films were stored in desiccator under vacuum for later use for measurement.

Considering an ideal mixture, approximate EO/Na ratio is calculated using the following equation[23]:

$$C = \left[\frac{M_{salt}}{\rho_{salt}} + \frac{EO}{Na}.\frac{M_{EO}}{\rho_{EO}}\right]^{-1} \quad \ldots (2)$$

where, M_{salt} and ρ_{salt} are the molecular weight (172 $gmol^{-1}$) and density (1.49 gcm^{-3}) of salt $NaCF_3SO_3$ respectively. M_{EO} is the molecular weight of EO unit (44 $gmol^{-1}$) and the density ρ_{PEO} is (1.1 gcm^{-3})[23,24]. X-ray diffraction analysis has been carried using Rigaku Miniflex model diffractometer instrument at ambient temperature. For impedance measurement, SOLARTRON-1260 Impedance/Gain-Phase Analyzer instrument has been used in the frequency range of 32 MHz - 1 Hz from ambient temperature to 338 K. The sample is placed between two blocking silver electrodes (dia. = 1.2 cm) under spring pressure for impedance measurements.

3 Results and Discussion

3.1 XRD analysis

Structural properties of a material depicting its crystalline nature, amorphous volume and crystallite sizes are studied using the XRD analysis. Diffractograms of the pure polymers and blend of the polymers without salt are shown in Fig. 1 and patterns for solid electrolyte samples are shown in Fig. 2. Calculated values of FWHM, average crystallite size, average inter-chainseparation and percentage of crystallinity are presented in Table 1.

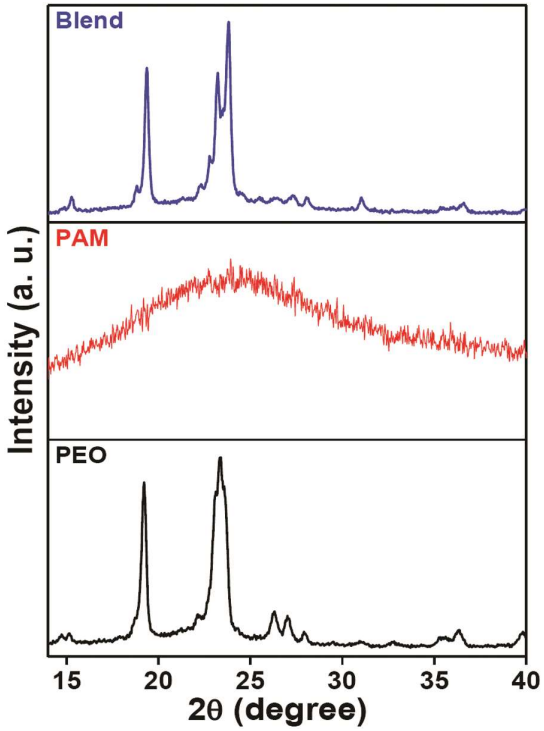

Fig. 1 – XRD patterns of pure PEO, PAM and blend sample without salt.

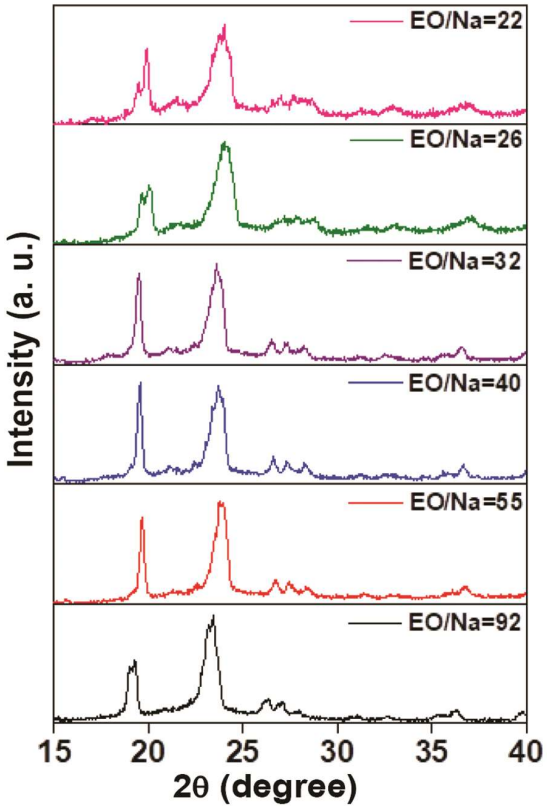

Fig. 2 – XRD spectra of electrolyte samples from EO/Na =92 to EO/Na =22.

Table 1 – XRD parameters and activation energies of pure PEO, pristine blend and blend electrolyte samples.

Sample	2θ (Degree)	FWHM β	L (nm)	R (Å)	% Crystallinity χ_c	Ionic conductivity (S/cm)	E_{ar} (eV)	E_{ac} (eV)
Pure PEO	19.22	0.32	0.4588	0.2824	67.30		-	-
	23.05	0.78	0.1931	0.2389				
Pristine Blend	19.47	0.39	0.3770	0.2868	62.13		-	-
	23.68	0.81	0.1869	0.2395				
EO/Na = 92	19.51	0.45	0.3268	0.2883	60.18	0.48×10^{-7}	0.80	0.77
	23.70	0.93	0.1628	0.2398				
EO/Na = 55	19.51	0.54	0.2728	0.2888	58.23	0.63×10^{-7}	0.79	0.79
	23.81	1.12	0.1357	0.2405				
EO/Na = 40	19.61	0.56	0.2624	0.2923	58.02	1.42×10^{-7}	0.82	0.82
	23.92	1.25	0.1250	0.2425				
EO/Na = 32	19.79	0.60	0.2445	0.2944	56.30	1.47×10^{-7}	0.79	0.79
	23.97	1.31	0.1109	0.2443				
EO/Na = 26	19.82	0.74	0.1991	0.2976	52.19	1.90×10^{-7}	0.77	0.75
	24.02	1.40	0.1084	0.2465				
EO/Na = 22	19.93	0.81	0.1828	0.2984	48.72	2.81×10^{-7}	0.70	0.69
	24.11	1.47	0.1030	0.2485				

Average crystallite size (L) is calculated using the Scherrer formula[25,26]:

$$L = \frac{k\lambda}{\beta cos\theta} \quad \ldots (2)$$

where, β is the FWHM of the peak (in radian), k is the shape factor whose value is assumed to be 0.9 for calculating the parameters and λ is the wavelength of Cu-K_α line = 0.154056 nm.

The average inter-chain separation is calculated using the following equation[27]:

$$R = \frac{5}{8}\frac{\lambda}{sin\theta} \quad \ldots (3)$$

The % crystallinity of the samples is calculated using the formula[28]:

$$\chi_c = \frac{A}{A_0} \times 100 \quad \ldots (4)$$

where, A is sum of areas of all crystalline peaks and A_0 is total area under entire diffractogram.

XRD patterns of pure polymers PEO, PAM and blend sample without salt are shown in Fig. 1. PAM shows only a broad hump at 2θ=25° indicating its amorphous nature. PEO shows crystalline peaks at 2θ=19° and 23°originating due to the orderings of poly ether side chains[29]. In the blend sample without salt, characteristic peaks of PEO at 2θ=19° and 23° are observed and no hump is seen due to PAM in the blend spectra.

Figure 2 shows diffractograms of blend electrolyte samples with varying EO/Na ratio. At 2θ=19° and 23°, slightly broadened but intense peaks, as seen in pure PEO spectra, are observed in all the electrolyte samples. As the salt is added, the intensity of peak at 19° gradually increases up to EO/Na = 40 and then after it starts decreasing and the width also increases. The X-ray peak at 19° splits and broadens for EO/Na = 32 and beyond, while at 23°, the peaks broaden. Small peaks beyond 25° are observed to be broadened for the electrolyte films. Peaks corresponding to $NaCF_3SO_3$ are not observed in the electrolyte samples which ascertain that the salt does not remain as an individual entity in the system. Overall alteration in the diffractogram patterns of pristine components, suppression of peaks and decrease in intensities and non-occurrence of salt peaks in the electrolyte system suggest structural reorganization of polymers and complete dissociation of salt in the system at the molecular level resulting in a good polymer-polymer and polymer-salt complexation[30]. From the above observations we can say that there is productive interaction amongst the constituent polymers which results in a miscible blend with traces of crystalline PEO.

Table 1 shows the values of various XRD parameters. Average crystallite size L and % crystallinity decrease with increase in salt concentration. Both the parameters indicate decrease in crystallinity with corresponding increase in amorphicity. Values of inter-chain separation R also increase with increase in salt content this leads to

increase in free volume of the system. Increase in free volume paves an easy conduction passage for mobile ion species leading to enhanced conductivity of the electrolyte system.

Apparent observations lead us to confirm the formation of a miscible blend electrolyte system which becomes more amorphous by successive addition of salt.

3.2 Ionic conductivity

Ionic conductivity of the blend electrolyte system was determined from complex impedance studies. Figure 3 shows Nyquist plots for the electrolyte samples at different concentrations of $NaCF_3SO_3$. Depressed semicircle in high frequency region and low frequency spikes with angle less than 90º are observed for all the samples. Intercept of semicircle on X-axis gives bulk resistance of the sample R_b. Then DC conductivity is found using the formula:

$$\sigma = \frac{1}{R_b} \times \frac{t}{A} \quad \ldots (5)$$

where, t is the thickness of the sample and A is the area of the blocking electrodes. As observed from the plots, value of R_b decreases with increase in salt concentration. This suggests that the conductivity of the electrolyte system increases with increasing salt. Calculated values of conductivity are presented in Table 1.

Figure 4 shows variation of conductivity as a function of frequency at various $NaCF_3SO_3$ concentrations. Three distinct regions are observed in the plots for all the electrolyte samples. Low frequency region is observed due to polarization at the electrode-electrolyte interface and mid frequency region is independent of frequency and is also called DC region observed due to diffusion of ions. In this frequency range, ions travel much faster and jump from one site to another available site. Successful hopping of ions to a neighboring vacant site contributes to the DC conductivity, when the frequency is lower than the hopping frequency (ω_p). In the third region, i.e., the high frequency region, the frequency exceeds hopping frequency(ω_p) and the conductivity continues to increase with increase in frequency. The crossover from frequency independent conductivity to dispersion depicts the relaxation phenomenon. Variation of hopping frequency can be interpreted in terms of charge carriers as:

$$\omega_p = \left(\frac{\sigma_{DC}}{A}\right)^{1/n} \quad \ldots (6)$$

where, σ_{DC} is DC conductivity of the sample, A is a constant for particular temperature and n is the power law exponent related to degree of interaction amongst mobile ions and lattice around them[31,32].The values of conduction activation energy E_{ac} are calculated from the values of ω_p and given in Table 1.

3.3 Dielectric studies

Permittivity of dielectric materials is the property used to measure the energy stored by them. Frequency dependent complex dielectric function ε* of a material is given as[33]:

$$\varepsilon^*(\omega) = \varepsilon'(\omega) - i\varepsilon''(\omega) = \frac{1}{i\omega C_0 Z^*} \quad \ldots (7)$$

Real and imaginary parts of complex impedance Z^* can be used to evaluate real and imaginary parts of the permittivity.

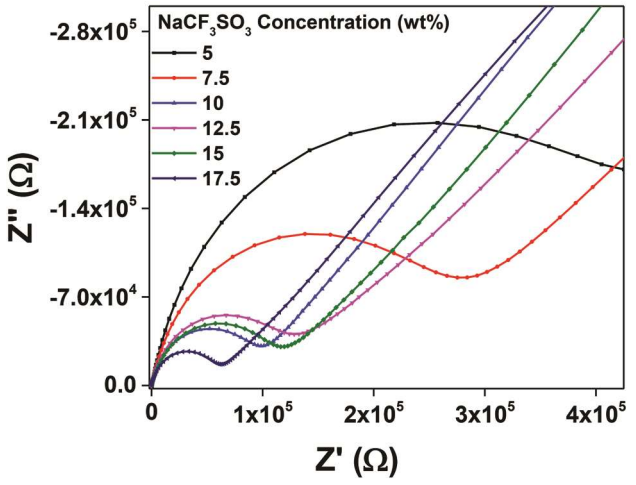

Fig. 3 – Nyquist plots for the electrolyte samples at different concentrations of $NaCF_3SO_3$.

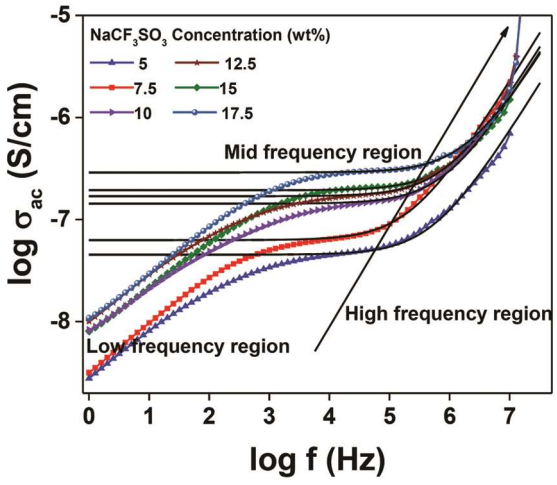

Fig. 4 – Variation of conductivity as a function of frequency at various $NaCF_3SO_3$ concentrations.

$$\varepsilon' = \frac{-Z_i}{\omega C_0(Z_r^2+Z_i^2)} \quad \ldots (8)$$

$$\varepsilon'' = \frac{-Z_r}{\omega C_0(Z_r^2+Z_i^2)} \quad \ldots (9)$$

where, $C_0 is$ the capacitance of the material in vaccum, ε_0 is the permittivity of free space and has the value of $8.854\times10^{-12}\,F/m$, $\omega = 2\pi f$ is the angular frequency and f is the frequency of the applied electric field. Real part of permittivity ε' corresponds to ordinary dielectric constant of the material which measures the amount of elastic energy stored in the material during every cycle of applied alternating field and the energy responded back to the field at the end cycle. Higher value of ε' suggests better conductivity. Figures 5 and 6, respectively, show frequency dependent ε' and ε'' at 323 K for different concentrations of $NaCF_3SO_3$.

Sharp increase in $\varepsilon'$and ε''at lower frequencies is observed due to the electrode polarization and space charge effects, which connote non-Debye behavior of the system[34]. The higher value of dielectric loss (ε'') at low frequency is observed due to the long distance charge motion within the materials. The appearance of peak is attributed to the relaxation phenomena of polymer. In low frequency region, dipoles are able to align themselves according to the electric field direction and hence contribute in the polarization process. At high frequencies both dielectric constant ε' and ε'' approach almost constant value. As the frequency is increased, the change in electric field becomes too fast for the charges to follow and hence, because of internal frictional forces, their contribution to the polarization approaches a small value[33]. As seen from Figs 5 and 6, the value of dielectric constant increases with increase in salt concentration and it is attributed to the increase in number of charge carriers with increasing amount of salt.

Figures 7 and 8, respectively, show frequency dependent ε' and ε'' plots for sample with 17.5 wt% $NaCF_3SO_3$ at different temperatures. The value of dielectric constant increases with increase in temperature. Applied electric field leads to formation of an electric moment inside the dielectric as a whole and also in each separate polarized molecule. These molecular dipoles cannot orient themselves at lower temperatures, increase in temperature favours the orientation of the dipoles and hence the value of dielectric constant increases[35].

3.4 Dielectric loss

Energy dissipation arising from charge transport and electrode polarization effect can be measured from dielectric loss. Electrode polarization occurs due to deposition of charges forming dipoles at the electrodes, which when applied by an electric field is forced to oscillate with the same frequency as that of applied field which leads to relaxation behavior similar to dipolar relaxation[36]. According to this convention, the deposited charges show a relaxation peak in dielectric loss spectra. Stevels[37], explained increase in dielectric loss as the relaxation phenomenon due to conduction losses, dipole losses and vibrational losses. Conduction losses rise with increase in temperature, which in turn causes the

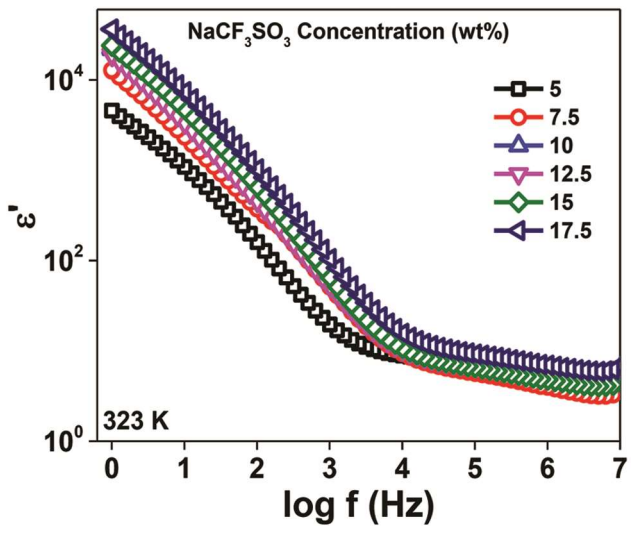

Fig. 5 – Frequency versus ε' plots with different salt concentration at 323 K.

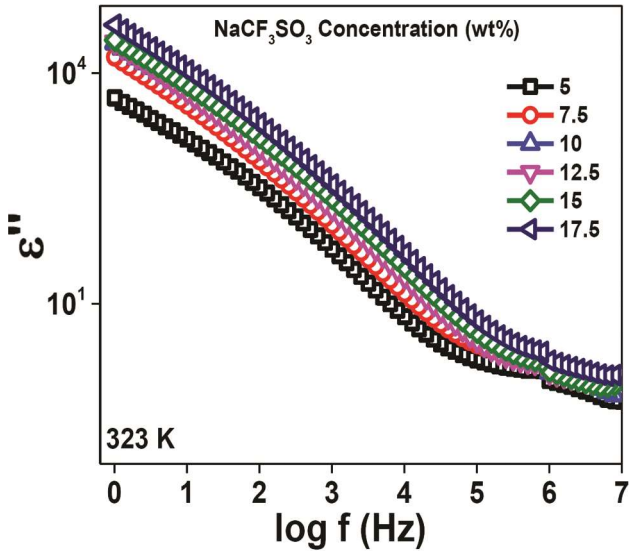

Fig. 6 – Frequency versus ε'' plots with different salt concentrations at 323 K.

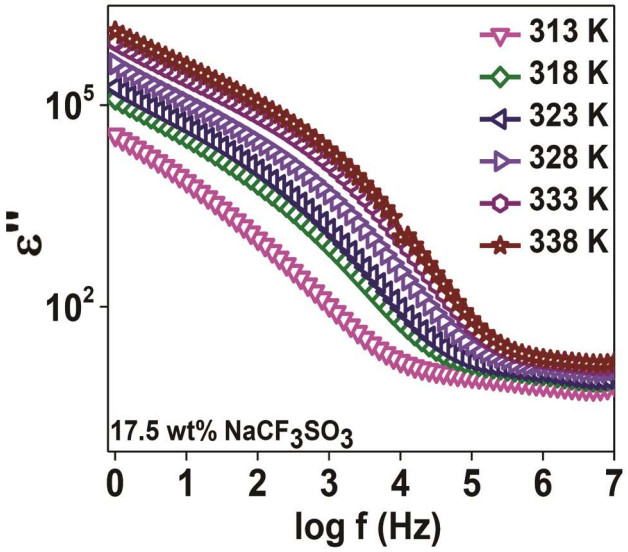

Fig. 7 – Frequency versus ε′ plots for sample with 17.5 wt% salt at different temperatures.

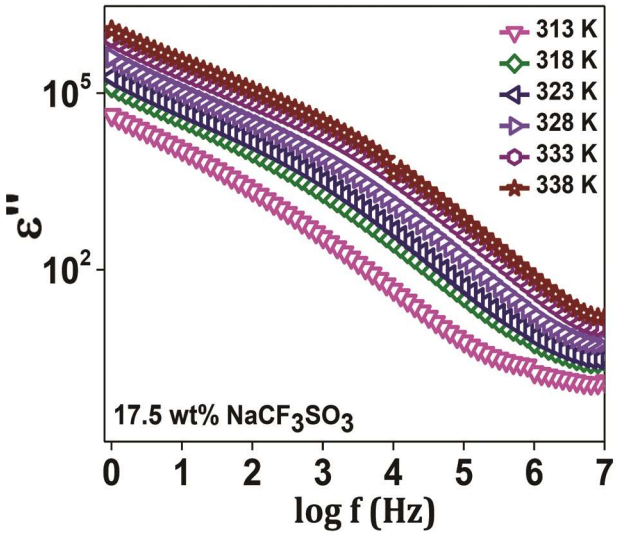

Fig. 8 – Frequency versus ε″plots for sample with 17.5 wt% salt at different temperatures.

value of dielectric loss to increase because conduction losses are proportional to (σ/ω). The tan δ peaks shift towards higher frequency side with successive addition of salt, i.e., relaxation time decreases. Figure 10 shows behavior of dielectric loss at various temperatures for sample with 17.5 wt% salt. From the plots, it is clear that tan δ value increases with frequency at different temperatures, passes through a maximum value and thereafter decreases and is attributed to ion jump and dc conduction loss of ions accompanied with polarization losses. Figure 10 shows that the frequency for relaxation peaks

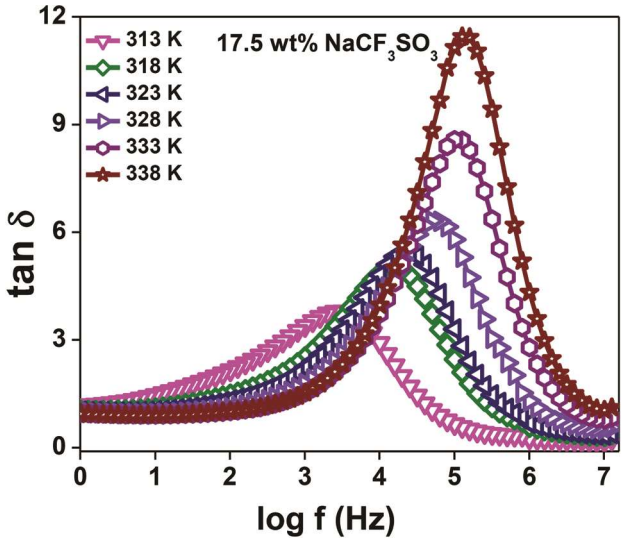

Fig. 9 – Frequency versus loss tangent at various salt concentrations.

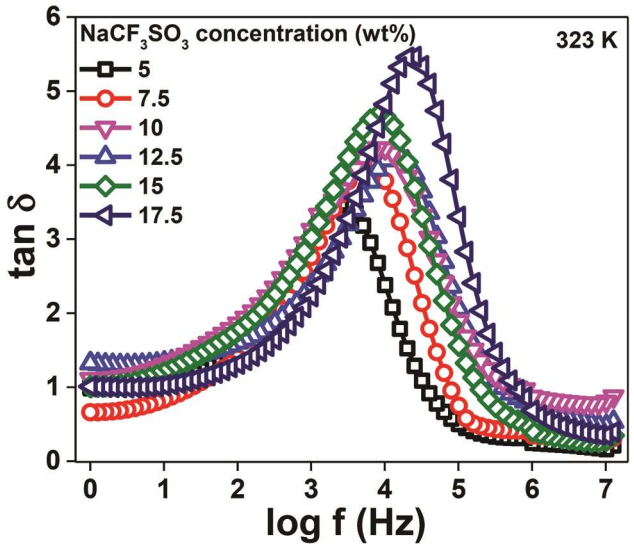

Fig. 10 – Frequency versus loss tangent for sample with 17.5 wt% salt at different temperatures.

increases with temperature and hence relaxation time decreases with increase in temperature. The decrease in relaxation time with increasing temperature is due to faster movement of sodium ions that synchronizes with the direction of applied field[30].

With increase in the salt concentration (Fig. 9), the magnitude of the loss increases and the loss peak shifts towards higher frequency side. The asymmetric shape of the (tan δ) peak around the maximum frequency (ω_{max}) suggests a deviation from classical exponential Debye behavior. The observed full width half maxima (FWHM) values of the tan δ peaks are found to be broader than the ideal Debye peak. The

relaxation time, $\tau=1/2\pi f_{max}$ can be calculated from the angular frequency ω_{max} at which the $(tan\delta)$ occurs. It is observed that the relaxation time decreases with increase in temperature as well as with the addition of sodium triflate.

3.5 Modulus studies

The dispersion behavior of the conductivity in the frequency domain is more conveniently interpreted in terms of conductivity relaxation time, τ using the electrical modulus, $M^* = {}^{1}/_{\epsilon^*}$ representation. Complex electric modulus M^* formalism is used very frequently when the relaxation behavior is presumed to be due to the motion of ions or electrons. Further information about the relaxation behavior of any electrolyte can be obtained from the complex electric modulus $M^*(f)$. The conductivity behavior can be conveniently interpreted in terms of conductivity relaxation time, τ in the frequency domain. Ionic conductivity is described by the modulus representation by associating a conductivity relaxation time with the ionic process.

Dielectric relaxation is due to the re-orientation process of dipoles in the polymer chains, which culminates into a peak in M''spectra.The real (M') and imaginary (M'') parts of $M^*(f)$ are calculated from the impedance data. Electric modulus is the electric counterpart of mechanical shear modulus; it corresponds to relaxation of electric field occurring at constant electric displacement[38]. Modulus studies are carried out to interpret the electrical relaxation processes occurring in the material which are difficult to distinguish from the polarization effect occurring at electrode-electrolyte interface. Macedo[39], presented the study of dielectric modulus to overcome this drawback. McCrum and others[40] in their book on polymeric solids have also suggested the use of modulus formalism. Ever since its discovery, modulus function has been used by researchers worldwide to understand and explain electrical relaxation phenomenon in different types of materials[41]. A comparison of the experimental data of $M^*$and $\boldsymbol{\varepsilon}^*$ is, therefore, useful to distinguish long-range conduction process from the localized dielectric relaxation.The dielectric response of modulus formalism M^* of a system is treated with complex permittivity ε^* by the following relationship[39-42]:

$$M^*(\omega) = \frac{1}{\varepsilon^*(\omega)} = M'(\omega) + jM''(\omega) = M_\infty[1 - \int_0^\infty \exp(-j\omega t)(-\frac{d\varphi(t)}{dt})dt] \quad \ldots (10)$$

where $M'$and M'' are the real and imaginary parts of the complex modulus M^*. The function $\varphi(t)$ gives the time evolution of the electric field within the material and $\omega = 2\pi f$ is the angular frequency.

Analysis of electrical relaxation in terms of complex permittivity $\varepsilon^*(\omega)$ gives relaxational parameters, characteristics of the decay of the displacement vector $\vec{D}$. The expression for the decay of electric field in time domain can be written as:

$$\vec{E}(t) = \vec{E}(0)\phi(t) \quad \ldots (11)$$

where $\vec{E}(0)$ denotes the electric field at time t=0 and $\phi(t)$ is a macroscopic decay function of the general form:

$$\phi(t) = \int_0^\infty g(\tau_\sigma)\exp\left[-\left(t/\tau_\sigma\right)^\beta\right]d\tau_\sigma \quad \ldots (12)$$

where $\tau_\sigma$is conductivity relaxation time, and $g(\tau_\sigma)$ is a normalized density function for relaxation times. Thus, using Eqs 10 and 12, it becomes:

$$M^*(\omega) = M_\infty\int_0^\infty g(\tau_\sigma)\left[\frac{j\omega\tau_\sigma}{(1+j\omega\tau_\sigma)}\right]d\tau_\sigma \quad \ldots (13)$$

Occurrence or absence of peak in frequency versus imaginary impedance plots is associated with space charge effects and non-localized conductivity. M''plots prove to be useful in understanding the behavior of the system when the relaxation processes are speculated to occur due to ionic motion and the electrode effects are suppressed. The plots of Z'' and M''as a function of frequency, Fig. 11(a) clearly show that the Z'' peak is developed at low frequency side while the peak for M'' is observed at higher frequency for 5wt% salt concentration. The Z'' peak shifts towards higher frequency side and reverse mechanism occurs for M'' spectra peak with the addition of sodium triflate in the blend as observed in Fig 11(b). Thus, it can be ascribed that the shift in peak frequency of M'' spectra suggests slower ionic motion in the system with the addition of salt. $Z''$and M''peaks do not appear at the same frequency which shows that the relaxation times are disseminated and the system shows non-Debye behavior[33]. Values of relaxation activation energy E_{ar} are calculated from the values of peak maxima of M'' spectra and presented in Table 1. It is noted from Table 1 that the values of conduction activation energies (E_{ac}) and relaxation activation energies (E_{ar}) are nearly same, this

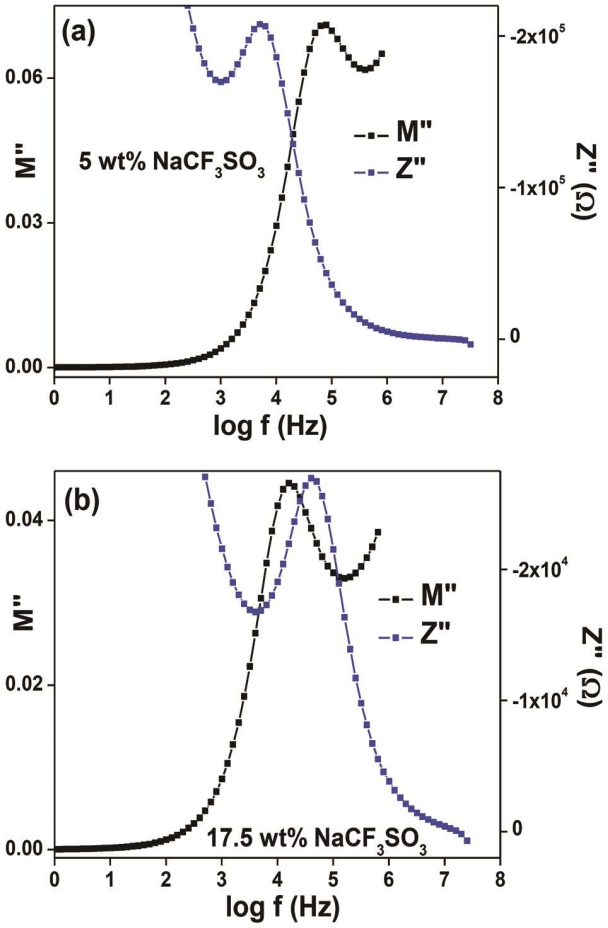

Fig. 11 – (a) Comparison of $Z''$and M'' spectra of samples with 5 wt% salt concentration and (b) comparison of $Z''$and M'' spectra of samples 17.5 wt% salt concentration.

suggests that the hopping mechanism dominates ion transport process in the present system and the ions encounter with equivalent barrier while relaxation and conduction processes[43]. This shows that the ionic and polymer segmental motion are strongly coupled.

Figures 12 and 13 show the modulus behavior of the system with frequency. Values of M' increase with increase in frequency and attain maximum value in higher frequency range. M''spectra show relaxation peak, which confirms the ionic nature of the material under study. The peak represents conductivity relaxation of the sodium ions in the system. Lower frequency side of the peak suggests long distance mobility of the charge carriers and the higher frequency side of the peak corresponds to caged movement of mobile ions[20]. The long tail appearing in the low frequency region is attributed to the large capacitance associated with the electrode polarization phenomenon[32]. Plots of M' and $M''$with frequency for

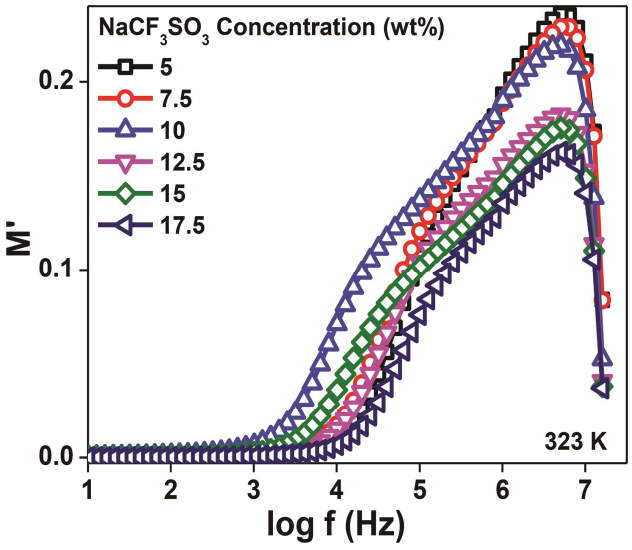

Fig. 12 – Frequency versus M′ plots with salt concentration at 323 K.

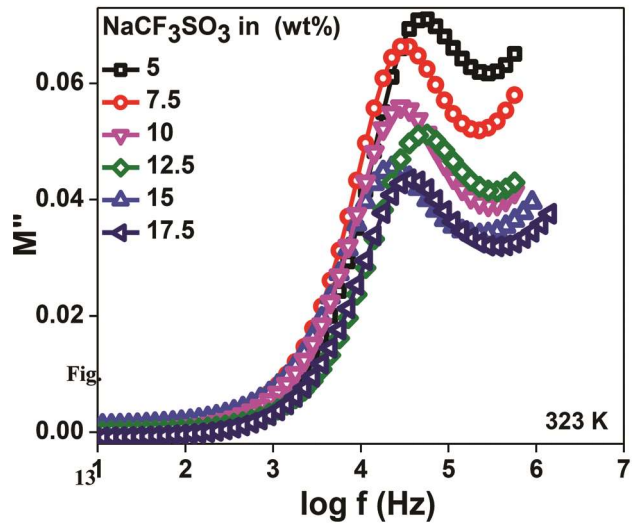

Fig. 13 – Frequency versus M″ plots with salt concentration at 323 K.

sample with 17.5 wt% salt concentration at various temperatures are shown in Figs 14 and 15. It is observed that M''plots display distinct relaxation peaks, which are related to the conductivity processes. The relaxation time decreases at higher temperatures due to faster ionic motion, hence the peaks shift towards higher frequency side[43].

The decay function $\phi(t)$ (in Eq. (12)) exhibits non exponential in amorphous systems i.e., if there is a distribution of relaxation times. In time domain, the decay function is called stretched exponential introduced by Kohlraush-Williams-Watts (KWW) and is given as:

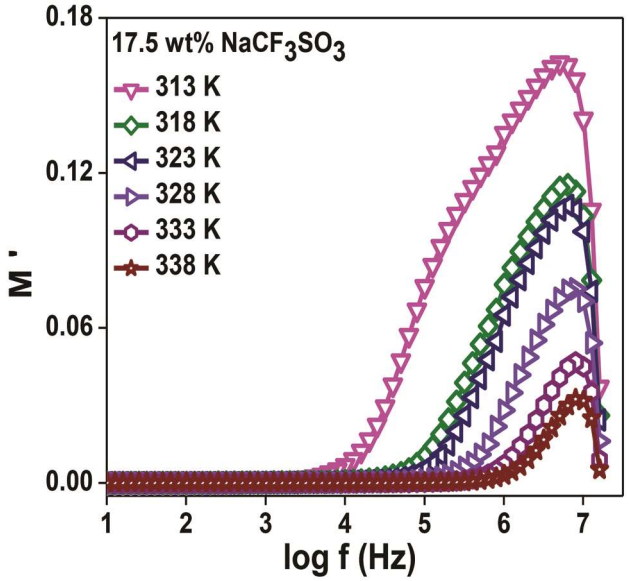

Fig. 14 – Frequency versus M′ plots for sample with 17.5 wt% salt concentration at different temperature.

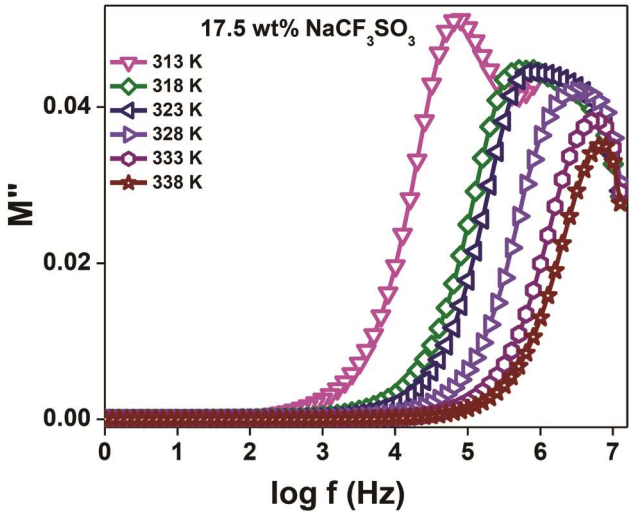

Fig. 15 – Frequency versus M″ plots for sample with 17.5 salt at different temperatures.

$$\phi(t) = \exp\left[-\left(\frac{t}{\tau_\sigma}\right)^{\beta}\right]; 0<\beta<1 \quad \ldots (14)$$

The asymmetric andout-spread shape of M'' peak can be approximated by stretched exponential Kohlraush-Williams-Watts (KWW) function[44] where, $\varphi_{KWW}(t)$ is the stretched exponential function of the electric field, t is the time and β is Kohlrausch-Williams-Watts exponent. The β parameter has been interpreted either as representatives of a distribution of relaxation times or as characteristic of cooperative motions between charge carriers. The relaxation

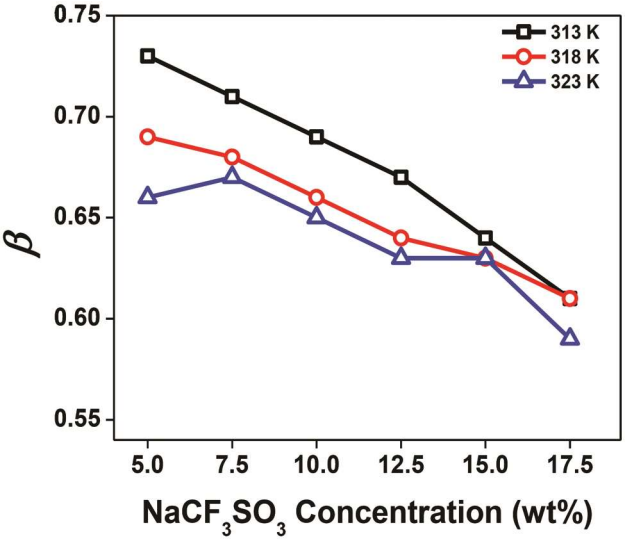

Fig. 16 – KWW parameter (β) versus salt concentration for different temperatures.

parameter, which increases with decrease in width of the relaxation time distribution and its values show the degree of deviation from ideal Debye behavior and β~0 illustrates maximum interaction between ions and the factors affecting the ion transport[29]. Calculated values of β for samples with varying salt concentrations at different temperatures are plotted in Fig. 16. β values decrease with increase in salt concentration as well as temperature. β values show a considerable deviation from Debye behavior and are in consonance with the results of $Z''$and M''vs $log\ f$ plots.

3.6 Scaling of modulus

Scaling of dielectric relaxation spectra is carried out to present whether the relaxation processes are independent/dependent of charge carrier concentration and/or thermally activated. Scaling provides a view into composition and temperature dependence of ion relaxation dynamics. We have used Ghosh's[45] scaling approach for scaling imaginary part of the modulus function. The scaling function is defined as:

$$\frac{M'}{M''} = F\left(\frac{f}{f_{max}}\right) \quad \ldots (15)$$

modulus M'' on y-axis is scaled by peak maximum value M''_{max} and frequency is on x-axis which is scaled by f_{max} which is the frequency of M''_{max}. Figure 17 shows scaling of M'' as a function of salt concentration. The M''plots do not merge onto a master plot but exhibit slightly different relaxation

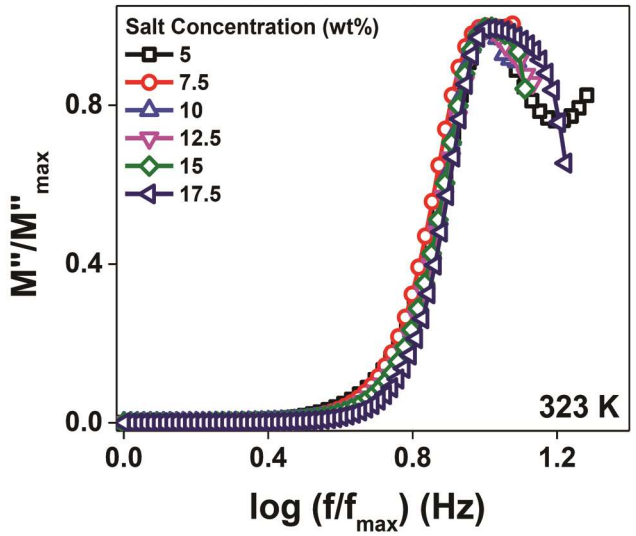

Fig. 17 – Scaling of M″ plots as function of temperature.

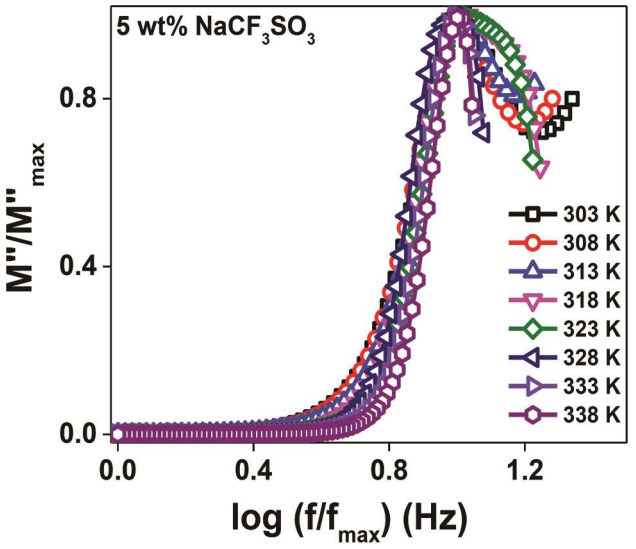

Fig. 18 – Scaling of M″ plots as function of salt concentration.

behaviour for different salt concentrations. Normalized plots do not form a perfect master curve which indicates that the relaxation process is dependent on salt concentration in the present electrolytes. Figure 18 shows scaling of M'' for sample with 17.5 wt% $NaCF_3SO_3$ at different temperatures. The scaled plots M''plots fail to fall into single master curve which indicates that the relaxation process are temperature dependent.

4 Conclusions

Dielectric relaxation and modulus studies of PEO-PAM based sodium salt electrolyte films prepared by solution cast technique were studied. Measured under identical experimental conditions, the films of [PEO:PAM]-$NaCF_3SO_3$ exhibit an enhanced dielectric response as compared to pure PEO:PAM. Dielectric loss increases with temperature. Stretched exponential decay and peaks in M'' spectra attribute the strong coupling between ionic and polymer segmental motions in the present ionic conductors. The value of dielectric constant increases with the increase in $NaCF_3SO_3$ salt in the electrolyte films and high conductivity indicates the usefulness of these films as a material for probable Na-solid polymer electrolytes. Relaxation process in PEO: PAM-$NaCF_3SO_3$electrolyte films is temperature as well as concentration dependent.

References

1 Wright P, *Electrochim Acta*, 43 (1998) 1137.

2 Kiran KK, Ravi M, Pavani Y, Bhavani S, Sharma AK & Rao V V R N, *Physica B*, 406 (2011) 1706.

3 Osman Z, Ansor N M, Chew K W & Kamarulzaman N, *Ionics*, 11(2005) 431.

4 Sivakumar M, Subadevi R, Rajendran S, Wu H C & Wu N L, *Europ Polym J*, 43 (2007) 4466.

5 Ramesh S, Leen K H, Kumatha K & Arof A K, *Spectrochim Acta A*, 66 (2007) 1237.

6 Rajendran S, Kannan R & Mahendran O, *Mater Lett*, 49 (2001) 172.

7 Radhakrishnan S & Venkatachalapathy P D, *Polymer*, 37 (1996) 3749.

8 Sumathi S, Sethuprakash V, Basirun W J, Zainol I & Sookhakian M, *J Sol-Gel Sci Technol*, 69 (2014) 480.

9 Virya A & Lian K, *Electrochem Commun*, 74(2017) 33

10 Fergus J W, *Solid State Ionics*, 227 (2012) 96.

11 Prasanth R, Shubha N, Hng H H & Srinivasan M, *Europ Polym J*, 49 (2013) 307.

12 Kim C S, Yoo J S, Jeong K M, Kim K & Yi C W, *J Power Sources*, 289 (2015) 41.

13 Kim S, Hana T, Jeonga J, Lee H, Ryoua M H & Lee Y M, *Electrochim Acta*, 241 (2017) 553.

14 Kumar D & Hashmi SA, *Solid State Ionics*, 181 (2010) 416.

15 Vignarooban K, Kushagra R, Elango A, Badami P, Mellander B E, Xu X, Tucker T G, Nam C & Kannan A M, *Int J Hydrogen Energy*, 41 (2016) 2829.

16 Hashmi S A & Chandra S, *Mater Sci Eng B*, 34 (1995)18.

17 Praveen D, Bhat S V & Ramakrishna D, *Ionics*, 19 (2013) 1375.

18 Kiran K K, Ravi M, Pavani Y, Sharma A K & Narasimha R V V R, *J Memb Sci*, 454 (2014) 200.

19 Fauteux D, Lupien M D & Robitaille C D, *J Electrochem Soc*, 134 (1987) 2761.

20 Marinov Y G, Hadjichristov G B, Petrov A G, Koduru H K, Marino L & Scaramuzza N, *IOP J Phys Conf Ser*, 794 (2017) 2020.

21 Véleza J F, Álvarez L V, Río C D, Herradón B, Mann E & Morales E, *Electrochim Acta*, 241 (2017) 517.

22 Wang C, Yeh Y, Wongittharom N, Wang Y, Tseng C, Lee S, Chang W S & Chang J K, *J Power Sources*, 274 (2015) 1016.

23 Devaux D, Bouchet R, Glé D & Denoyel R, *Solid State Ionics*, 227 (2012) 119.

24 Fetters L J, Lohsey D J & Colbyz R H & Mark J E, *Physical properties of polymers handbook*, 2nd Edn, (Springer: New York), (2007) 447.

25 Cullity B D & Stock S R, *Elements of X-ray diffraction*, 3rd Edn, (Prentice Hall: New Jersey) (2001) 99.

26 Raghu S, Subramanya K, Ganesh S, Nagaraja G K & Devendrappa H, *Radiat Phys Chem*, 98 (2014) 124.

27 Alexander L E, *X-ray Diffraction methods in polymer science*, (John Wiley: New York) (1969) 379.

28 Kumar A, Saikia D, Singh F & Avasthi D K, *Solid State Ionics*, 177 (2006) 2575.

29 Sharma P, *Study of conduction mechanism in PEO-PMMA polymer blend nano-composite electrolytes*, Ph D Thesis, The Maharaja Sayajirao University of Baroda, 2013.

30 Pradeepa P, Edwinraj S & Ramesh P M, *Chin Chem Lett*, 26 (2015) 1191.

31 Jonscher A K, *Nature*, 267 (1977) 673.

32 Pant M, Kanchan D K & Gondaliya N, *Mater Chem Phys*, 115 (2009) 98.

33 Sharma P, Kanchan D K & Gondaliya N, *Ionics*, 19 (2013) 777.

34 Navaratnam S, Ramesh K, Ramesh S, Sanusi A, Basirun W J & Arof A K, *Electrochim Acta*, 175 (2015) 68.

35 El-Nahass M M, El-Deeb A F, El-Sayed H E A & Hassanien A M, *Physica B: Condens Matter*, 388 (2007) 26.

36 Coelho R, *Revue Phys Appl*, 18 (1983) 137.

37 Stevels J M & S Flugge, *Handbuch der physik*, Edn, (Springer: Berlin), (1957) 350.

38 Molak A, Paluch M, Pawlus S, Klimonko J, Ujma Z & Gruszka I, *J Appl Phys*, 38 (2005) 1450.

39 Macedo P B, Moynihan C T & Bose R, *Phys Chem Glasses*, 13 (1972) 171.

40 Mc Crum N G, Read B E & Williams G, *Anelastic and dielectric effects in polymeric solids*, (Dover: New York) 1991.

41 Hodge I M, Ngai K L & Moynihan C T, *J Non-Cryst Solids*, 351 (2005) 104.

42 Tapabrata D, Satya T, Marian P, Sidhartha S J & Dillip K P, *Electrochim Acta*, 202 (2016) 147.

43 Das S & Ghosh A, *Electrochim Acta*, 171 (2015) 59.

44 Gondaliya N, Kanchan D K, Sharma P & Joge P, *J Appl Polym Sci*, 125 (12) 1513.

45 Karmakar A & Ghosh A, *Curr Appl Phys*, 12 (2012) 539.